AIAA 82-4063

Laser Doppler Velocimeter Measurements on Supersonic Mixing Nozzles that Employ Gas-Trips

August A. Cenkner Jr.*
Bell Aerospace Textron, Buffalo, N.Y.

A cold flow laser Doppler velocimeter study was performed in the mixing region of supersonic mixing nozzles that employed gas-trips for enhanced mixing; the nozzles were operated with room-temperature nitrogen under simulated laser flow conditions. A determination was made of three mean and turbulent velocity components, in addition to two turbulent shear stress elements, under both trip-on and trip-off operation. To preclude velocity biasing, the primary, secondary, and trip streams were simultaneously seeded with 0.357-μm-diam latex spheres. The objectives of this activity were to acquire basic cold flow information on trip nozzles in order to help develop some insight into the tripped mixing phenomenon and to acquire information that could be correlated with sophisticated computer models of the mixing process. The velocimeter results appear to support observations that were made earlier during a related laser-induced fluorescence visualization study.

Introduction

IN many combustion devices (e.g., chemical rocket and jet engines, lasers) unmixed reactants are independently fed via adjacent mixing nozzles into a reaction chamber, where mixing and chemical reactions occur. It has been found that the mixing phenomenon has a significant effect on the performance of the device. Gas-trips have recently been installed in various mixing nozzles in an attempt to enhance mixing and thereby improve device efficiency. With this approach, gas is injected through small orifices that are located in the nozzles near the exit plane in an attempt to "trip" the flow; that is, as one theory goes, trigger premature transition from laminar flow.

The use of gas-trips in the cavity mixing nozzles of chemical lasers has resulted in more than a doubling of the laser power. Infrared radiometer scans of the mixing region have verified that the power increase was due to enhanced reactant mixing.[1] While a number of theories have been proposed to explain this enhanced mixing, evaluation of these theories has been frustrated by a lack of extensive experimental information. Because of this, a cold flow experimental project was initiated on chemical laser nozzles that employ gas-trips. The primary objective of this activity was to acquire basic gasdynamic information on supersonic trip nozzles, under simulated laser flow conditions, to help develop some insight into the trip-enhanced mixing phenomenon.

Earlier in this program, testing was conducted on four different supersonic slit nozzle arrays that utilized gas-trips. Included were extensive pitot probing and flow visualization studies using laser-induced fluorescence of selectivity seeded iodine vapor.[2]

In this phase of the program, the mixing region of a BCL-10 trip nozzle array was probed with a laser Doppler velocimeter (LDV). In addition to satisfying the primary program objective, a secondary goal of the LDV phase was to acquire information that could be correlated with sophisticated computer models of the mixing process.[3-5] Hence, measurements were made of three mean and turbulent velocity components, as well as two turbulent shear stress elements, under both trip-on and trip-off cold flow operation.

A considerable amount of gasdynamic research has been performed in the past with an LDV. However, no work has been conducted with trip nozzles and Ref. 6 appears to be the only attempt at working with laser nozzles. This activity was directed toward acquiring a limited number of hot reacting flow measurements on an HF chemical laser, using a chemical seeding technique. The type of LDV that was employed appeared to suffer from spatial resolution limitations.

BCL-10 Trip Nozzle

A small nozzle array that utilizes the BCL-10 laser nozzle design was fabricated specifically for the cold flow study. As can be seen in Fig. 1, the 1.27×1.27 cm array has four secondary and three primary nozzles; gas-trip orifices are visible in the left blade of each nozzle. All trips are fed through two tubes from a common cylindrical reservoir located above the top of the nozzle block. Four tubes are used to feed the secondaries from a common cylindrical reservoir located below the bottom of the nozzle block. A 1.746 cm i.d. tube served as a common backfeed for all the primary nozzles, thereby simulating the flow from a laser combustor.

Supply pressures and flow rates are independently controlled in the primary, secondary, and trip circuits. The primary and secondary plenum pressures are measured at the inlets to the 1.746 cm feedline and the cylindrical reservoir, respectively. While the trip (supply) pressure is measured at the inlet to the cylindrical trip reservoir, this does not correspond to the plenum condition upstream of the trip orifices. This is because of orificing inside the nozzle block. The nozzle operating point is given in Table 1. Calibrated sonic orifice flowmeters were used for all flow measurements.

For all tests, the nozzle array was centered in an 8.89 cm i.d. cylindrical test section. This was to insure free-jet operation of the jet array.

Details on the high-pressure supersonic BCL-10 wedge nozzle profiles are given in Fig. 2. For discussion purposes, the secondary nozzles of Fig. 1 are designated from left to right: S1, S2, S3, and S4. The primaries are numbered in a similar fashion.

Figure 3 gives details on the gas-trip orifice pattern. In general, there are six trip orifices in the left blades and seven in the right blades of each nozzle. No orifices were placed in the outside blades of the two outside secondary nozzles (S1 and S4). All the secondary orifices are 0.0102 cm in diameter while the primaries are 0.0178 cm. Since the trip holes in the left nozzle blades are staggered relative to the right blades, the orifices are numbered. From top to bottom, the sequence for the left blades of the primaries (and secondaries) would run

Received April 20, 1981; revision received May 18, 1981.

*Scientist, High Energy Laser Technology. Member AIAA.

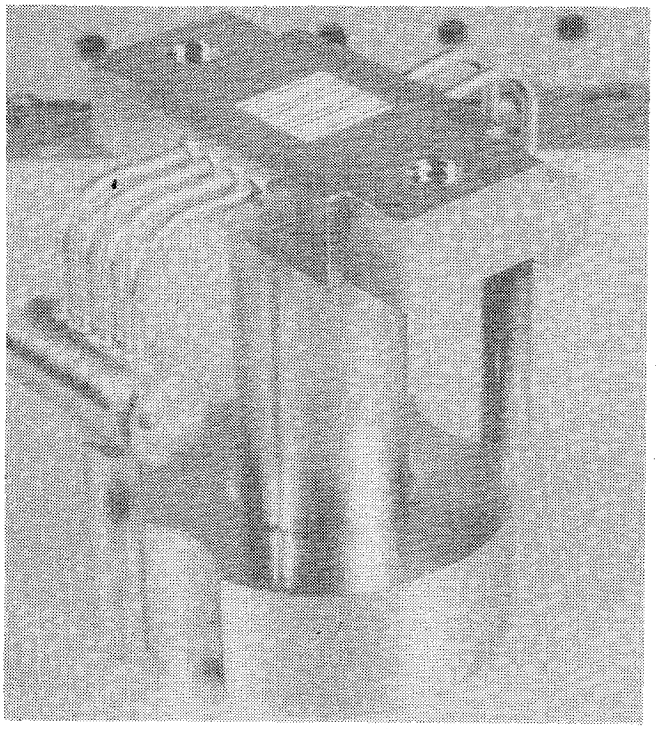

Fig. 1 BCL-10 laboratory nozzle array.

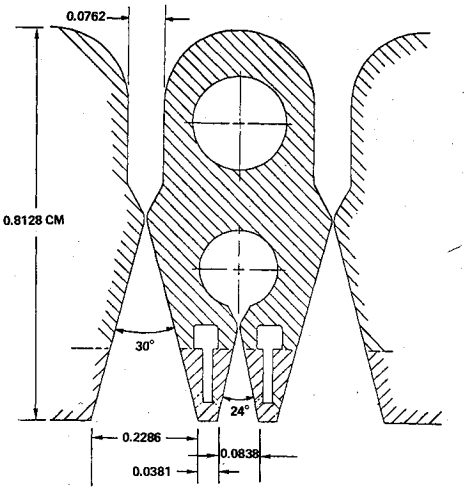

NOZZLE	PRIMARY	SECONDARY
NUMBER	3	4
THROAT WIDTH	0.0076 CM	0.0076 CM
GEOMETRIC AREA RATIO	30	11

Fig. 2 BCL-10 nozzle contour.

Table 1 BCL-10 laboratory test conditions

Primary nozzle	
Plenum pressure	746 kPa
Plenum temperature	20°C
Flowrate	4.54 g/s
Gas	Nitrogen
Secondary nozzle	
Plenum pressure	253 kPa
Plenum temperature	20°C
Flowrate	1.50 g/s
Gas	Nitrogen
Gas-trips	
Supply pressure[a]	400 kPa
Supply temperature	20°C
Flowrate	0.473 g/s
Gas	Nitrogen
Cavity	
Cavity pressure	2 kPa

[a] Upstream of distribution orifice in nozzle.

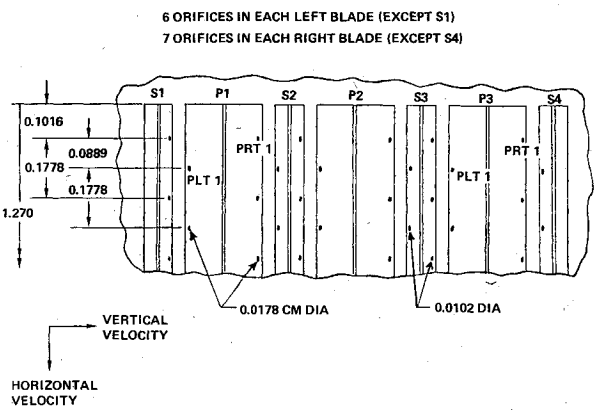

Fig. 3 BCL-10 trip orifice locations.

from PLT1 to PLT6. Notice in Fig. 2 that the trip orifices are inclined at 45 deg relative to the nozzle centerline.

Laser Doppler Velocimeter

A unique laser Doppler velocimeter was developed by Bell Aerospace Textron (BAT) specifically for making velocity and turbulence measurements in the mixing region of small chemical laser nozzles.

Two factors proved to be the driving considerations in the design of the system. First, it was desired to measure supersonic turbulent velocities where the mean velocity could exceed 3000 m/s. Second, the measurement volume had to be small enough so that reasonable spatial resolution could be achieved. An appreciation for the severity of the latter requirement can be gained by considering the characteristic dimensions of the BCL-10 chemical laser trip nozzle in Figs. 2 and 3. These considerations dictated the need for a single-burst system that would respond to Doppler frequencies as high as 300 MHz. BAT undertook the development of a special high-frequency signal processor when it became apparent that such a capability was not commercially available.

The developed LDV can be characterized as a 320 MHz (Doppler frequencies up to 320 MHz can be measured), two-color (two different color laser beams are used so that two velocity components can be measured simultaneously), off-axis (collects forward scattered radiation off the axis of the focused laser beam), single-burst system (the velocities of single particles are measured as they individually pass through the measurement volume). In the two-color arrangement of Fig. 4, each integrated optical cell is used to split/transmit/focus one color beam while simultaneously receiving the forward scattered light of the opposite color beam. The measuring volume formed by each set of transmitted laser beams is essentially an elongated ellipsoid. When the two ellipsoids intersect, the spatial resolution is defined by the region that is common to both. Advantages of this type of arrangement, beyond that of a small probe volume, are that two velocity components can be detected simultaneously from a single particle passing through the probe volume and the signal-to-noise ratio is greatly improved. The data acquisition equipment consists of two photomultiplier tubes, a signal processor, and a system minicomputer with its associated teletype, CRT histogram display, data rate counter, and magnetic tape storage unit.

The light scattered by particles suspended in the flow is converted to an electrical format by the photomultiplier tubes

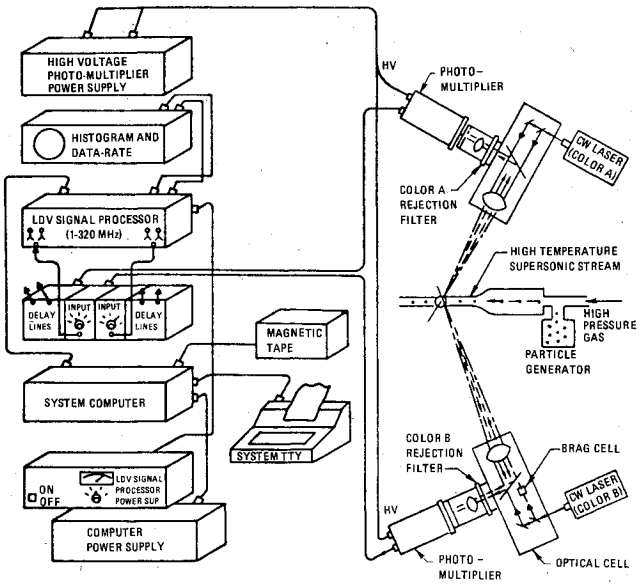

Fig. 4 Schematic of two-color, off-axis, 320 MHz, single-burst laser Doppler velocimeter (LDV).

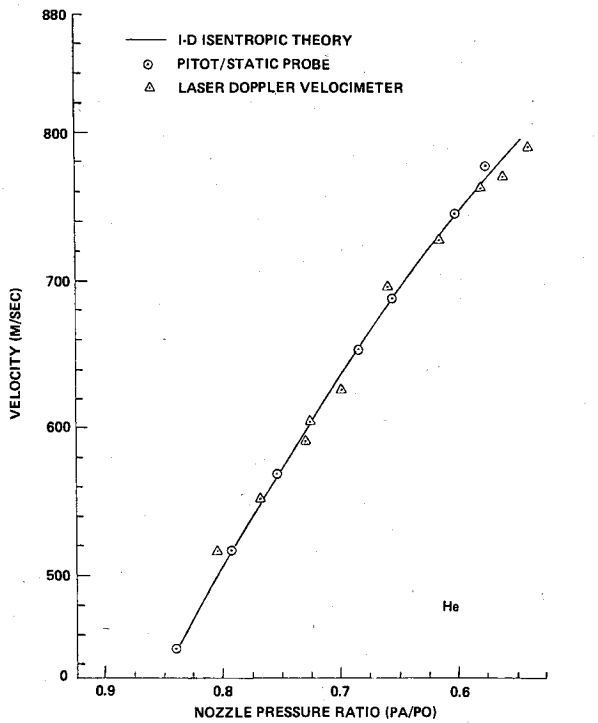

Fig. 5 Laser Doppler velocimeter checkout using an atmospheric free jet (converging axisymmetric nozzle).

and fed to a dual-channel signal processor. The basic function of this instrument is to measure the Doppler frequency of the single-particle bursts, perform quality checks on the signal, and if the signal quality is acceptable, feed a digitally formated analog of the two measured frequencies to the minicomputer. When a statistically meaningful number of single-particle measurements are recorded at a given point in the flowfield, the data set is automatically transferred to a magnetic tape for off-line statistical analysis. The system is then reset so that it is ready to be commanded to accept the next data set. A counter displays either the rate at which single-particle measurements are being made or the total number of accumulated single-burst measurements. The computer is also used for generating a real-time CRT histogram display of a single data set.

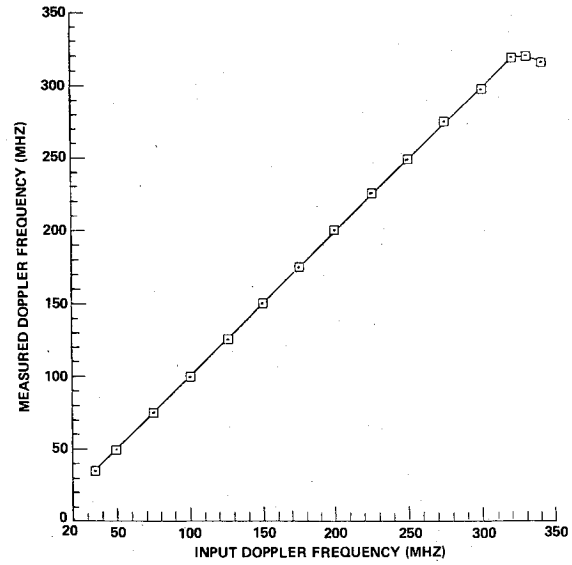

Fig. 6 Measured frequency response of 320 MHz LDV signal processor.

During checkout of the LDV, an atmospheric helium free jet was first used for correlating LDV mean velocity measurements (out to 800 m/s) with those obtained with a pitot/static probe and theoretical one dimensional (1-D) isentropic predictions (see Fig. 5). All measurements were made in the core region of the jet close to the face of a converging axisymmetric nozzle. Gas velocity was increased by increasing the plenum pressure while maintaining the back pressure at atmospheric conditions. Three-way disagreement is less than 2%. A supersonic nitrogen free jet was then used to study low-pressure performance. With an axisymmetric converging/diverging nozzle, operating on-design with a 2 kPa back pressure, there was less than a 4% disagreement between 1-D isentropic predictions of the centerline mean velocity (668 m/s) and the measured LDV value. During the next LDV checkout phase, an electrical Doppler burst simulator was used for testing the signal processor over its entire range. From Fig. 6, there was about a 0.50% disagreement between the measured frequencies and the inputed frequencies, out to 320 MHz.

In light of the theoretical predictions of Yanta,[7] a 1000 particle data set was selected for all checkout and testing. With a 1000 particle set, it is predicted that there is a 95% confidence level that there will be about a 1% error in the computed mean velocity for a 15% turbulent intensity. Similarly, there is a 95% confidence level that the computed standard deviation is in error by less than 4%.

Seeding

Three atomization-type particle generators were developed for seeding hot and cold turbulent supersonic flows with submicron particles. An electron microscope served for performance characterization with solid titanium dioxide, alumina, and spherical latex particles. Mean particle sizes and gasborne concentrations were determined as a function of suspension concentration and carrier gas flow rate for both helium and nitrogen carrier gases. The generator has been operated up to 4 h without any noticeable degradation in performance. During this study, the three generators were installed in such a way that all three gas streams could be seeded simultaneously.

Test Procedure

The nozzle test section was mounted directly to a milling machine so that the test section could be translated accurately in three dimensions relative to the fixed LDV measurement

volume. Dial indicators gave the relative positions of the measurement volume once an origin was established. The LDV electro-optical subsystem was mounted on a stationary optical bench in close proximity to the test section. During the test, the seeding system was also mounted directly on the bench as close as possible to the test section. The air legs of the bench were not pressurized during this work. Testing indicated that vibration pickup through the legs would produce a slight broadening of the histogram. The broadening was judged tolerable and of less concern than run-to-run repeatability in positioning the measurement volume.

With the chemical laser gas-trip nozzle of interest, test gases are independently fed to the primary and secondary nozzles as well as the trip orifices. These gases interact in some unknown fashion in the laser cavity mixing region. To prevent biasing of the LDV measurements, all three test gases must be seeded with particles simultaneously. Since the test gases have different supply pressure requirements, three independently controlled particle generators were required. The need for independent seeding of the three gas streams can be better understood by considering the operating principle of a single-burst LDV. Each time an acceptable particle passes through the measurement volume, its velocity is measured. When a sufficient number of these single particle velocities are recorded, enough so that the sample forms a statistically meaningful histogram, the flow parameters can be determined statistically from the sample. In the mixing region, the primary, secondary, and trip streams are interacting in some unknown manner and could be contributing particles to each sample. Failure to simultaneously seed all three streams would result in an undetected biasing of the histogram and the computed flow parameters.

Latex spheres, with diameters of 0.357 μm and a standard deviation of 0.0056 μm, were selected as the seeded particles. They were initially suspended in alcohol. No attempt was made to remove the alcohol vapor from the flow as it did not appear to adversely affect the operation of the LDV or the nozzle. For compatibility with the nozzle working fluid, nitrogen was used as the carrier gas. A charge neutralizer, cyclone, and seven-stage impactor were used in all generators to minimize the number of coagulated particles. Particles were seeded into each feed circuit through a small tube that was centered in each feedline. To minimize the affect of resulting flow disturbances on nozzle performance, the injection points were installed about 5 ft upstream of the nozzle.

Single-channel LDV operation was first selected for direct measurement of the axial velocity component at three axial stations that were 0.76, 1.52, and 2.29 cm from the nozzle face; the measurement volume was essentially centered between the PLT4 and the PRT4 trip orifices. At a given axial location, the flow was first traversed with trip-off nozzle operation and then with trip-on operation. To assess repeatability, two consecutive data sets were frequently acquired at some nodes. Elapsed time between single-node consecutive data sets was typically about 20 s. During this test sequence, the nozzle slits were oriented horizontally, while traversing was performed vertically.

Three-component velocity measurements were then taken at the 0.76 cm axial station, using the X-fringe technique discussed in Ref. 8. This method allows for the determination of turbulent shear stress, in addition to two components of the mean and turbulent velocities. To perform three-component velocity measurements, it was necessary to rotate the nozzle. Vertical and axial components were found with the nozzle slits oriented horizontally; traversing was vertical. Horizontal and axial components were then determined with the nozzle rotated so that the nozzle slits were vertical; traversing was now horizontal.

For all work reported herein, each data set was comprised of 1000 consecutive single-particle velocity measurements. Node spacing was set at 0.0127 cm. All traversing was done in such a way that the measurement volume moved parallel to the nozzle face. A 150 MHz low-pass external filter was used during all testing in order to eliminate high-frequency histogram biasing by electrical noise. Since the highest measured Doppler frequency was about 120 MHz, there was no filtering of the Doppler signal.

Two approaches were used in analyzing the data. Normal statistical relationships were first used. Accordingly, the mean and turbulent (root-mean-square) velocities are computed from

$$\bar{u} = \frac{1}{N} \sum_{i=1}^{N} u_i \tag{1}$$

$$u_{\text{rms}} = \sqrt{(u')^2} = \sqrt{\frac{1}{N} \sum_{i=1}^{N} (u_i - \bar{u})^2} \tag{2}$$

where N is the sample size at each node = 1000.

The second approach used the weighting factor proposed by McLaughlin and Tiederman[9] for computing the mean velocity. The weighting factor corrects for biasing due to the fact that faster particles will be sampled more frequently than slower particles. The mean velocity relationship therefore becomes

$$\bar{u} = \sum_{i=1}^{N} u_i \left(\frac{1}{u_i}\right) \Big/ \sum_{i=1}^{N} \left(\frac{1}{u_i}\right) \tag{3}$$

It was found that there was less than a 1% disagreement between these two approaches, possibly because of the low turbulence that was encountered. All of the mean and turbulent velocities reported herein were computed by the standard statistical relationships given in Eqs. (1) and (2).

In selecting the components of the optical cells, the major consideration was to minimize the dimensions of the measurement volume so that reasonable spatial resolution could be achieved. The selected components had the following characteristics:

$\lambda = 0.488$ μm, laser beam wavelength
$w = 28$ mm, beam spacing
$D = 1.408$ mm, $1/e^2$ diameter of blue beam
$F = 440.5$ mm, focal length of focusing lens
$N_f = 32$ fringes, number of fringes in ellipsoidal volume
$d_e = 0.0244$ cm, minor axis diameter of ellipsoid
$l_e = 0.7645$ cm, major axis diameter of ellipsoid

The length of the ellipsoidal volume (l_e) is obviously too large for meaningful results. To reduce this dimension to an acceptable size, off-axis collection was employed. With a small aperture in front of the photomultiplier (PM) tube and optimized selection of the collection optics, it was found that with

$d_a = 0.0102$ cm, diameter of aperture in front of PM tube
$F_a = 200$ mm, focal length of scattered light focusing lens
$F_c = 289.0$ mm, focal length of collecting lens

we get

$l_e' = 0.0566$ cm, effective length of measurement volume

The effective width of the measurement volume is somewhat less than the minor axis diameter because of signal checks made by the LDV signal processor. The LDV only requires 12 fringe crossings by a particle, while there are actually 32 fringes in the ellipsoidal volume. Therefore,

$d_e' = 0.0076$ cm, effective width of measurement volume

To assess spatial resolution capabilities, a comparison is now made between several characteristic dimensions of the

BCL-10 nozzle and the measurement volume size. From Figs. 2 and 3, the secondary nozzle width is 0.0838 cm, the base width is 0.0381 cm, and the centerline-to-centerline spacing of the trip orifices is 0.0889 cm. These dimensions compare to a measurement volume length of about 0.0566 cm and a width of 0.0076 cm.

Discussion of Results

Mean and turbulent axial velocity data that were acquired at the 0.76, 1.52, and 2.29 cm axial stations are given in Figs. 7-12. Consider first the trip-off behavior. Near the nozzles, at 0.76 cm, an inviscid core can be detected in both the primary and secondary trip-off streams. At this location, the centerline velocity of the primary stream is only about 7% higher than that of the secondary stream, despite the fact that the primary area ratio is 175% greater. This is because the velocity is asymptotically approaching the theoretical limit. Moving from the 0.76 to the 1.52 cm station, the width of the secondary profile increases and that of the primary profile shrinks, while both centerline velocities increase. At the 2.29 cm station, the centerline secondary velocity has dropped, while the primary centerline velocity remains unchanged; both profiles are reduced in width. This complex jet interaction is related to viscous, pressure, and three-dimensional effects—the latter being, no doubt to a large extent, related to side feeding of the secondary nozzles and mismatches in nozzle exit pressures and the back pressure. Inasmuch as there

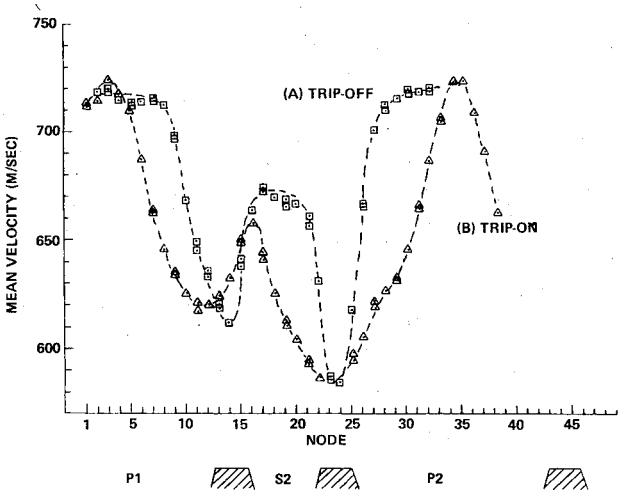

Fig. 7 Mean axial velocity, 0.76 cm.

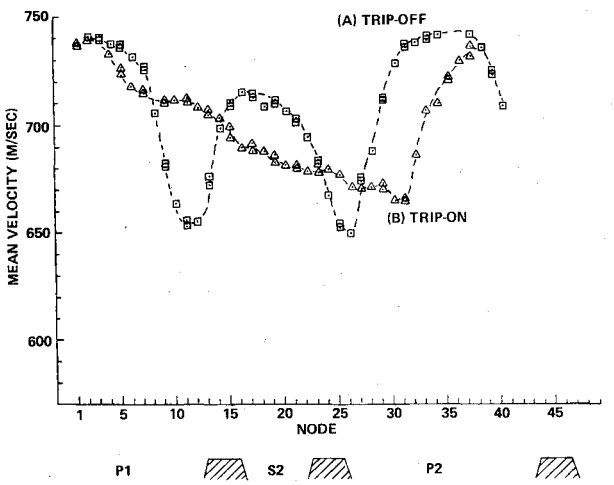

Fig. 8 Mean axial velocity, 1.52 cm.

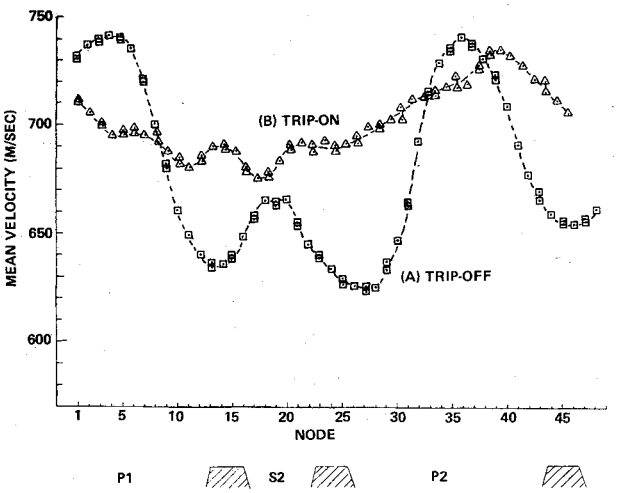

Fig. 9 Mean axial velocity, 2.29 cm.

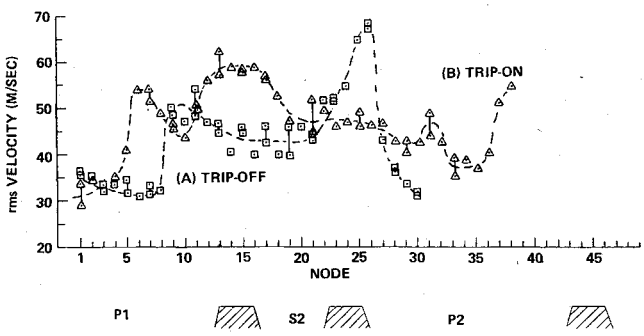

Fig. 10 Turbulent axial velocity, 0.76 cm.

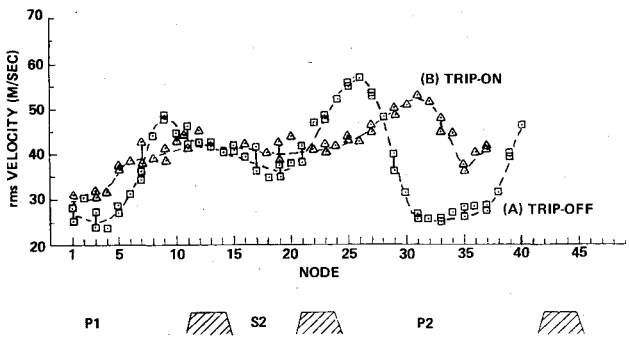

Fig. 11 Turbulent axial velocity, 1.52 cm.

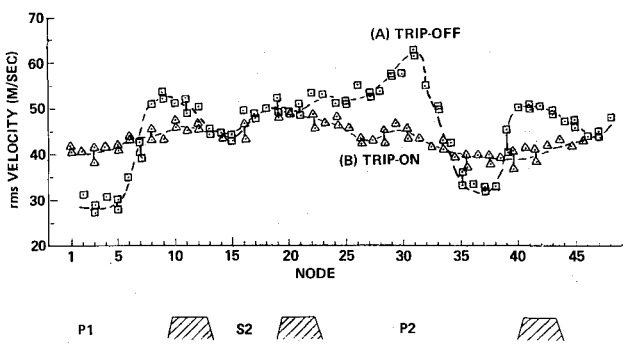

Fig. 12 Turbulent axial velocity, 2.29 cm.

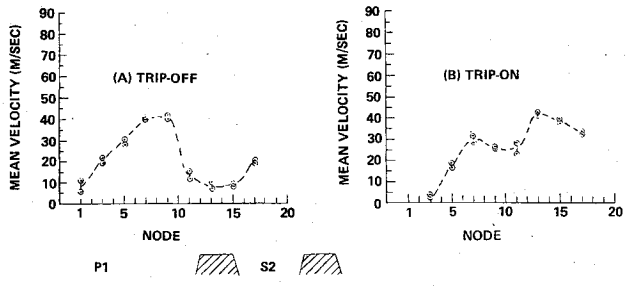

Fig. 13 Mean vertical velocity, $\bar{v}$, 0.76 cm.

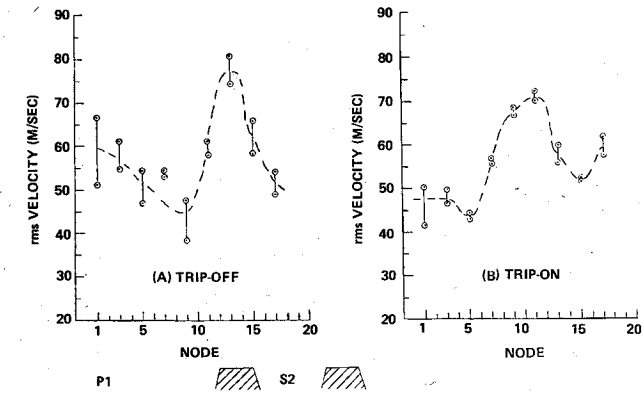

Fig. 14 Turbulent vertical velocity, v_{rms}, 0.76 cm.

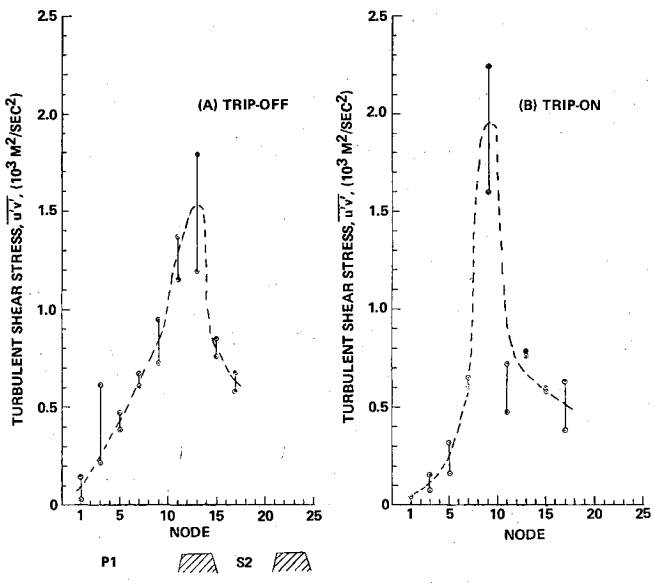

Fig. 15 Vertical turbulent shear stress, $\overline{u'v'}$, 0.76 cm.

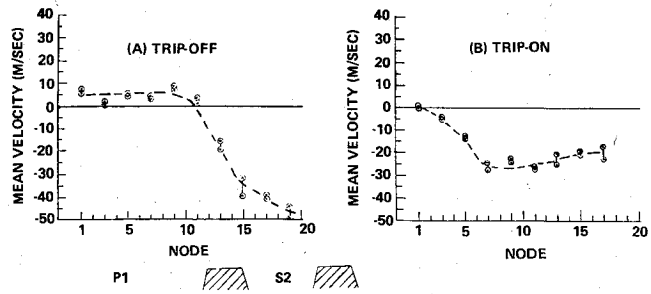

Fig. 16 Mean horizontal velocity, $\bar{w}$, 0.76 cm.

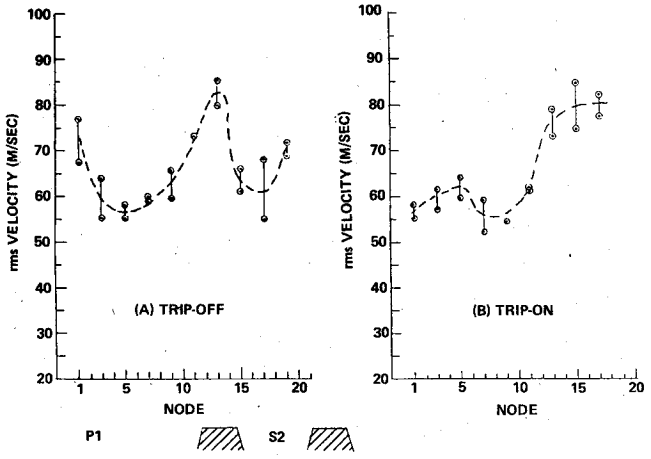

Fig. 17 Turbulent horizontal velocity, w_{rms}, 0.76 cm.

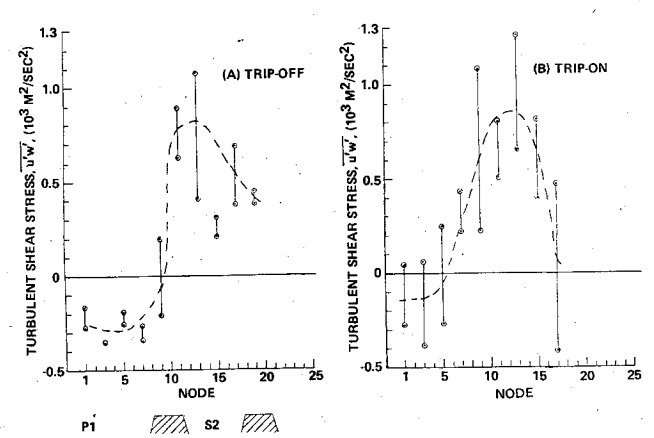

Fig. 18 Horizontal turbulent shear stress, $\overline{u'w'}$, 0.76 cm.

is about twice as much of an increase in the centerline secondary velocity as compared to the primary velocity, between the 0.76 and 1.52 cm locations, the increase does not appear to be due to an undetected zero shift in the LDV. A velocity deficit in the wakes of the P1/S2 and S2/P2 bases can be clearly identified at all three axial locations.

When the trips are turned on, two phenomena occur at 0.76 cm. The primary and secondary profiles both narrow considerably and the S2 jet shifts leftward. At 1.52 cm, the trip-on behavior gives the impression that the S2 jet has been distorted and shifted leftward. To attempt an interpretation of these results, it is necessary to digress somewhat. As was demonstrated by the earlier flow visualization work of Ref. 2, near the nozzle face the trip jets behave in many ways like solid, deformable bodies. They are solid bodies in the sense that they retain their identities as discrete entities, thereby displacing regions of the main flow and altering the original pressure distribution. They are deformable bodies in the sense that their size, shape, and location are dependent upon operating conditions. The trip jet cross-sectional shape has been observed to sometimes appear crescent shaped and to sometimes resemble the letter "U" or "H." Further downstream from the nozzle, these jets break up and intermix with the main flow; complete breakup of the primary and secondary trip jets occurs at different axial locations. From the above discussion it follows that the leftward shift at 0.76 and 1.52 cm could be due to the (solid body) trip jets displacing the secondary gas. Narrowing of the primary and secondary jets could then be related to viscous interaction with the lower velocity trip jets and/or a local compression of these jets. The mean velocity behavior at 2.29 cm may then

reflect trip jet breakup.

Consider now the trip-off turbulent velocities for the same region of the flowfield that was considered above; see Figs. 10-12. As would be expected, at 0.76 cm the turbulence peaks in the high shear wakes of the P1/S2 and S2/P2 bases. The turbulent velocity on the secondary centerline is about 50% higher than that on the primary centerline, no doubt because of the differences in nozzle widths. Moving downstream to 1.52 and 2.29 cm, the turbulence zone spreads further into the primary stream and the secondary core turbulence increases; however, there is very little change in peak turbulence and the turbulent intensity (rms/mean velocity) never exceeds about 10%. The turbulence distribution always remains nonuniform over the entire width of the flow and the lower turbulence primary core persists out to the farthest axial station. Notice that the P1/S2 and S2/P2 wakes are nonsimilar at all three axial locations. By comparing Figs. 7-9 and Figs. 10-12, it can be seen that, as the turbulence spreads with increasing axial location, the mean jet velocities start to drop off. This is because the high-speed kinetic energy of the flow is being converted into turbulence (and then into internal energy) in the high shear wake regions.

At 0.76 cm, when the trips are turned on, the peak of the P1/S2 turbulent wake is shifted leftward from nodes 9-10 to node 6; the S2/P2 wake is broadened and also shifted from node 26 to nodes 14-15. Curiously, at 1.52 cm, the peak of the S2/P2 wake, at first glance, appears to shift rightward from node 26 to node 31. However, a closer examination reveals that this may not be the case. Observe in the trip-on scan of Fig. 10 that there appears to be the start of a local turbulence zone at node 31. The more intense and wider region that was observed downstream at node 31, in Fig. 11, may actually be this newly established zone. At the final downstream location of Fig. 12, the turbulence is spread more uniformly over the entire flowfield, but the peak turbulence has not increased. This turbulence behavior also appears to be consistent with the solid body trip jet explanation that was discussed above. The entire explored trip-on and trip-off region has a relatively low level axial intensity of less than about 10%.

Both the trip-on and trip-off mean vertical velocities (defined in Fig. 3) are relatively low level (Fig. 13), with the maximum being only about 5% of the P1 axial centerline velocity. Flow from the P1 jet moves from the P1 centerline toward the P1/S2 wake. This is to be expected since a source flow wedge nozzle design was used. Flow into the secondary stream may be due to a mismatch between the primary and secondary exit pressures and/or side feeding of the secondary nozzles. The trip-off peak turbulence (Fig. 14) is almost double that of the maximum mean velocity. When the trips are turned on, there is no dramatic increase in peak turbulence. Rather, the turbulent (trip-off) wake shifts leftward and expands somewhat. The turbulent shear stress profile also shifts leftward somewhat, when the trips are turned on in Fig. 15.

From Fig. 16 it can be seen that under trip-off operation there is little, if any, horizontal flow in the primary stream (Fig. 16). However, a measurable velocity does develop in the secondary jet. This component may also be due to a mismatch between the nozzle exit pressure(s) and the cavity pressure, or side feeding of the secondaries. As with the vertical component, the turbulent velocity exceeds the mean velocity (Fig. 17). When the trips are turned on, the mean velocity zone spreads while the peak velocity drops off. The horizontal turbulent shear stress zone of Fig. 18 appears to be somewhat wider than the vertical shear zone of Fig. 15.

Conclusions

Mean and turbulent velocities were measured in the mixing region of a BCL-10 slit nozzle array under both trip-on and trip-off operation. Key observations can be summarized as follows:

1) The flowfield is three-dimensional, even under trip-off operation. This is no doubt related to a mismatch in nozzle exit and cavity (back) pressures, and to side feeding of the secondary nozzles.

2) The gas trips do not enhance the turbulence in the (trip-off) wake regions. Rather, the trips locally spread the turbulence into the adjacent lower turbulence regions.

3) The LDV results appear to be consistent with the flow visualization work that shows that the trip jets act like solid, deformable bodies near the nozzle.

4) The trip-on and trip-off axial turbulent intensity is low level, being no more than 10% at peak locations.

5) The peak vertical and horizontal turbulent velocities exceed their respective mean velocities.

6) The trip-off secondary nozzles are filled with higher levels of turbulence sooner than the primary nozzles. This is probably related to differences in the widths of these nozzles.

7) The trip-off centerline velocity of the secondary stream drops off faster than that of the primary stream.

8) The LDV measurement volume is small enough so that localized flow phenomenon can be resolved.

Acknowledgments

The author would like to express his appreciation to G. W. Tregay and R. J. Driscoll for discussions and suggestions that were related to nozzle testing and to a review of the original manuscript. The author would also like to acknowledge assistance in the development of the LDV that was given by L. Moon, E. Clune, S. Martin, T. Lang, and D. Marshall. This work was supported under Air Force Contract F29601-77-C-0007 while development of the LDV was supported under corporate IR&D funding.

References

[1] Gross, R.W.F. and Bott, J. F., *Handbook of Chemical Lasers*, John Wiley and Sons, New York, 1976.

[2] Cenkner, A. A. Jr. and Driscoll, R. J., "Laser Induced Fluorescence Visualization on Supersonic Mixing Nozzles that Employ Gas-Trips," *AIAA Journal*, to be published.

[3] Mellor, G. L. and Herring, H. J., "A Survey of the Mean Turbulent Field Closure Models," *AIAA Journal*, Vol. 11, May 1973, pp. 590-599.

[4] Bradshaw, P., "The Understanding and Prediction of Turbulent Flow," *Aeronautical Journal*, Vol. 76, No. 739, July 1972, pp. 403-418.

[5] Ramshaw, J. D. and Dukowicz, J. K., "Apache: A Two-Dimensional Reactive Fluid Dynamics Code for Chemical Laser Applications," LA-UR 78-2765, Los Alamos Scientific Laboratory, Los Alamos, N. Mex., 1978.

[6] Hackett, C. E., "Laser Velocimetry Measurements in the Cavity of HF Chemical Laser," SAND76-9314, Sandia Laboratories, Albuquerque, N. Mex., Feb. 1977.

[7] Yanta, W. J., "Turbulence Measurements with a Laser Doppler Velocimeter," NOLTR-73-94, Naval Ordnance Laboratory, Silver Spring, Md., May 1973.

[8] Yanta, W. J., "Laser Doppler Velocimeter Measurements of Turbulence Properties of a Mach 3 Turbulent Boundary Layer," *Proceedings of the Second International Workshop on Laser Velocimetry*, Vol. I, March 1974, p. 115.

[9] McLaughlin, D. K. and Tiederman, W. G., "Biasing Correction for Individual Realization of Laser Anemometer Measurements in Turbulent Flows," *Physics of Fluids*, Vol. 16, Dec. 1973, pp. 2082-2088.